Preliminary Design of the SHMS Noble Gas Čerenkov Detector

Donal Day
University of Virginia
Charlottesville, VA

1 Introduction

The use of Čerenkov detectors for particle identification is a well established technique in nuclear and particle physics. They are nearly ubiquitous as part of detector packages in magnetic spectrometers and together with shower counters, Čerenkov detectors serve to identify the charged particles passing through the momentum acceptance of the spectrometer. As part of the 12 GeV upgrade at Jefferson a new spectrometer, the Super High Momentum Spectrometer (SHMS) will be built in Hall C.

Analyzing momenta up to 11 GeV/c at scattering angles from 5.5 to 40.0 degrees, the SHMS will reach kinematic regions in which the pion background rate dominates the scattered electron rate by more than 1000:1. The suppression of these anticipated pion backgrounds while maintaining efficient identification of electrons is therefore one of the main duties of the SHMS detector elements and the SHMS Noble Gas Čerenkov Detector shoulders a large portion of this particle identification burden. Here I report the preliminary design choices for a noble gas threshold Čerenkov detector that will meet these twin goals of suppression and identification.

2 Choice of Gases

The basic equation[1] governing Čerenkov radiation emitted by a particle of velocity β travelling through a medium with index of refraction n is

$$\cos\theta = \frac{1}{\beta n}, \tag{1}$$

where θ is the angle of the Čerenkov light cone. From this it is easy to see that for there to be any radiation

$$n > 1/\beta.$$

What we need is that

$$n < 1/\beta_{\pi,max} \tag{2}$$

to guarantee that the pions produce no radiation directly, and that

$$n > 1/\beta_{e^-,min} \tag{3}$$

to guarantee that all the electrons produce Cerenkov light. Since $1/\beta_{e^-,min} < 1/\beta_{\pi,max}$, we need to use only one value of n over the planned momentum range. Figure 1 emphasizes this point with a plot of the hadron velocity (given as $(1-\beta)$) as a function of momentum along with the lines indicating the index of refraction of various gases at 1 atm, as $(n-1)$. For a threshold Cerenkov counter only those particles with $(1-\beta) < (n-1)$ will produce light. For example no π's with momenta greater than 6 GeV will.

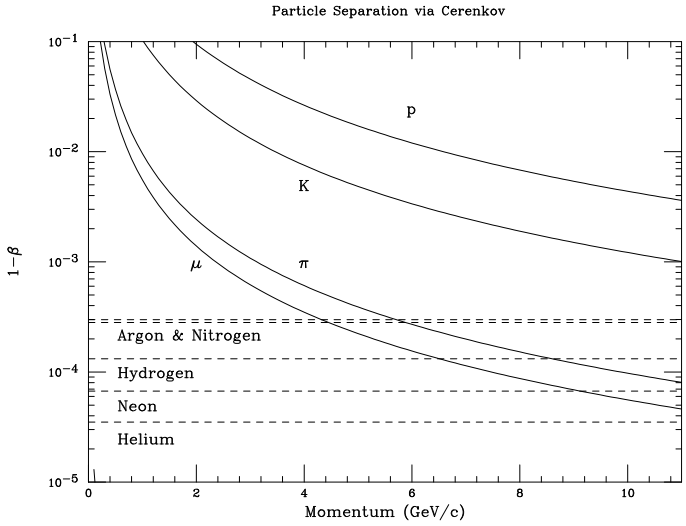

Figure 1: Particle identification with a threshold Cerenkov detector. Plotted is the hadron velocity as $(1-\beta)$ against the hadron momenta. The horizontal lines indicate, for different gases at 1 ATM, the index of refraction as $(n-1)$. Only when $(1-\beta)$ is less than $(n-1)$ does the particle produce light.

For gases, we also have the relationship between the pressure and index of refraction[2]: $P = (n-1)/k$, where k is a gas dependent factor. Table 1 lists several gases and their k values. To satisfy Equation 2, we get

$$P_{max} = \frac{1-\beta_{\pi,max}}{\beta_{\pi,max}k}. \tag{4}$$

These values are listed in Table 1. A first glance indicates that neon would be a good choice for the SHMS Cerenkov detector. At 1 atm will allow the windows on the detector tank to be as thin as possible.

It is also possible to use a mixture of gases to fine tune the index of refraction and improve the detector performance. In this case the weighting of the index of refraction of the different gases is by the number of molecules per unit volume

for each gas and the index is linear in the number per unit volume for each species. It should be possible to obtain pre-mixed gases from a vendor or mix them using techniques already in use at the laboratory.

Gas	k	$P_{max}^{6\ \mathrm{GeV/c}}$	$P_{max}^{10\ \mathrm{GeV/c}}$
Helium	.238	7.73	2.30
Neon	.456	4.04	1.20
Hydrogen	.939	1.96	0.58
Oxygen	1.85	0.99	0.30
Dry Air	1.86	0.99	0.29
Argon	2.21	0.95	0.28

Table 1: Possible gases for use in SHMS Cerenkov. P_{max} is the maximum pressure in ATM for which a 6 (10) GeV/c pion will remain below threshold. $k = (n-1)/14.7$.

3 Photoelectron Production

For a particle of charge e, we have the following relationship[2] for the radiated energy per unit path length and unit frequency:

$$\frac{dE}{dxd\omega} = r_e m(1 - \frac{1}{\beta^2 n^2})\omega,$$

r_e is the classical electron radius. Expressing the above in terms of wavelength, we have

$$\frac{dE}{dxd\lambda} = 4\pi^2 r_e mc^2 \frac{1}{\lambda^3}(1 - \frac{1}{\beta^2 n^2}). \tag{5}$$

Now we can write down the number of photons N produced as

$$\frac{dN}{dxd\lambda} = 2\pi\alpha\frac{1}{\lambda^2}(1 - \frac{1}{\beta^2 n^2}), \tag{6}$$

α being the fine structure constant. Note that the photon production grows as $1/\lambda^2$.

We can convert this into the number of photoelectrons, N_e, produced with the relationship

$$dN_e = \epsilon_c(\lambda)\mathrm{QE}(\lambda)\mathrm{G}(\lambda)dN, \tag{7}$$

where $\epsilon_c(\lambda)$ is the light gathering efficiency of the detector; $\mathrm{QE}(\lambda)$, the quantum efficiency of the photomultiplier tube (PMT); $\mathrm{G}(\lambda)$, the transparency of the gas. Doing this conversion, we have

$$dN_e = 2\pi\alpha(1 - \frac{1}{\beta^2 n^2})\epsilon_c(\lambda)QE(\lambda)\mathrm{G}(\lambda)\frac{d\lambda}{\lambda^2}dx. \tag{8}$$

If we (correctly) assume that n is constant over the interval λ_1 through λ_2, we can express the total number of photoelectrons as

$$\begin{aligned} N_e &= \int_0^L \int_{\lambda_1}^{\lambda_2} 2\pi\alpha(1-\tfrac{1}{\beta^2 n^2})\epsilon_c(\lambda)QE(\lambda)\mathrm{G}(\lambda)\tfrac{d\lambda}{\lambda^2}dx \\ &= 2\pi\alpha(1-\tfrac{1}{\beta^2 n^2})\int_{\lambda_1}^{\lambda_2}\epsilon_c(\lambda)QE(\lambda)\mathrm{G}(\lambda)\tfrac{d\lambda}{\lambda^2}\int_0^L dx \\ &= AL(1-\tfrac{1}{\beta^2 n^2}) \end{aligned} \tag{9}$$

where

$$A = 2\pi\alpha\int_{\lambda_1}^{\lambda_2}\epsilon_c(\lambda)QE(\lambda)\mathrm{G}(\lambda)\frac{d\lambda}{\lambda^2}. \tag{10}$$

The factor A now contains all the detector design specific parameters, including the choice of PMT and radiator gas (with respect to absorption).

4 Estimates on A

The integral $A = 2\pi\alpha\int_{\lambda_1}^{\lambda_2}\epsilon_c(\lambda)QE(\lambda)\mathrm{G}(\lambda)\frac{d\lambda}{\lambda^2}$ can be numerically evaluated. If we assume that the light will only bounce once off one the mirrors, $\epsilon_c(\lambda)$ can be approximated by knowing the reflectivity efficiency of a thin aluminum coating (see Figure 2). QE(λ) is taken from the specifications for different PMTs[1]. An example of the $QE(\lambda)$ can be seen in Figure 3 where it is shown for three different samples of the Hammamatsu R1584 which has a bialkali photocathode and UV glass.

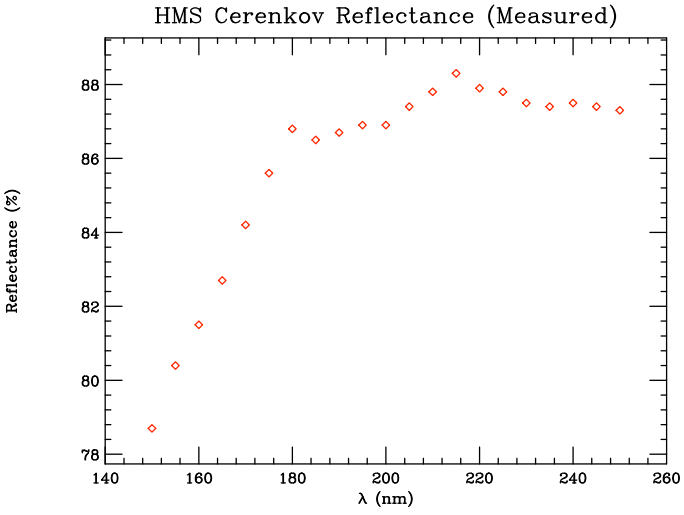

Figure 2: Reflectance of one of the HMS Cerenkov mirrors manufactured at CERN.

[1]In the estimates I used 80% of the manufacturer's listed values of $QE(\lambda)$ to account for inefficiencies in the collection of the electrons emitted from the photocathode.

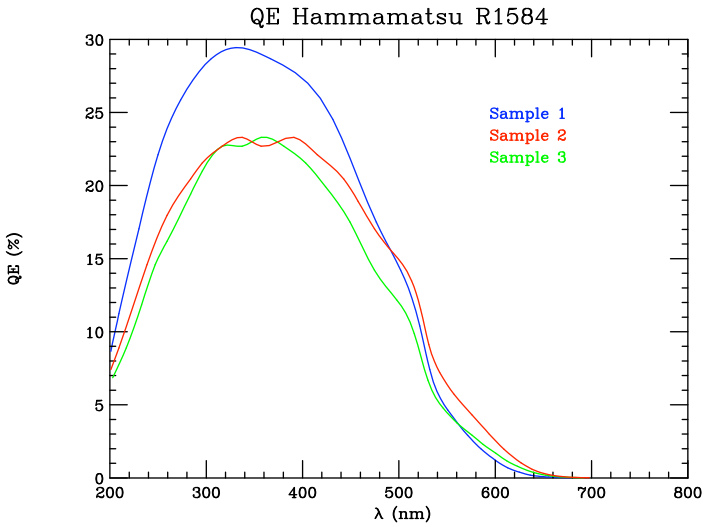

Figure 3: Quantum efficiency for the Hammamatsu R1584 5 inch PMT. The behavior as a function of wavelength is typical of most tubes. Note the difference in the QE for the three different samples tested. $QE(\lambda)$ data provide by Hammamatsu.

The transparency $G(\lambda)$ for the noble gases (which we plan on using) is taken to be 1.0 over the entire range of λ.[2] The results for 5 in diameter PMTs are listed in Table 2 where I have taken a 240 cm long volume of Neon at 1 atm with an index of refraction $n = 1.000067$.

Company	Tube	Size (in)	λ_1 (nm)	λ_2 (nm)	A cm^{-1}	N_e
Burle	8854	5	185	630	142	4.6
Hamamatsu	R1836	5	160	650	299	9.6
Hamamatsu	R1584, green	5	185	650	161	5.2
Hamamatsu	R1584, red	5	185	650	176	5.7
Hamamatsu	R1584, blue	5	185	650	215	6.9

Table 2: Estimates of A and N_e for a 240 cm Neon volume at 1 atm (11 GeV pion threshold) for various PMTs using 80% of the manufacturer's claim for QE and assuming no absorption. The Burle tube is no longer available and the Hamamatsu R1836 has a quartz window. The three entries for the R1584 refer to the three different samples in Fig. 3.

The optics of the SHMS Čerenkov Detector will employ four spherical mirrors and four photomultiplier tubes (see Section 5). The mirrors will have a front-reflecting surface of vacuum deposited aluminum, protected by a layer of MgF, on a 3 mm thick, 155 cm radius of curvature, 40 cm by 40 cm glass substrate. To minimize any bending of the mirrors whose concave size faces the target,

[2]This is due to their large ionization potentials.

tilted at angle of 15 degrees with respect to the vertical, the mirrors will be glued to a stiff foam material, Rohacell [3].

The Hammamatsu phototubes (R1584) we have chosen have a 5 inch diameter UV glass entrance window, a bialkali photocathode with high quantum efficiency. Unfortunately it lacks a high gain GaP(Cs) first dynode as the Burle 8854 in the HMS Čerenkov which makes it easier to distinguish the single photoelectron peak.

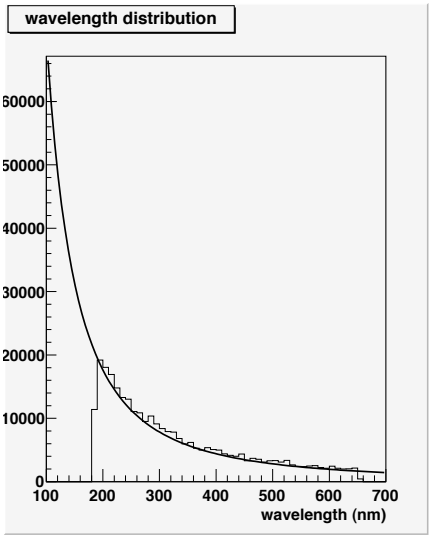

Figure 4: Distribution of the wavelengths of the Cerenkov photons from the Geant4 simulation (See Section 5.1.) along with a fit.

The Geant4 simulation (See Section 5.1.) provides the wavelength of the photons produced which goes as $\frac{1}{\lambda^2}$ and for which we provide the distribution in Figure 4. By taking this distribution along with the quantum efficiency given in Figure 3 for the blue line, we find the average quantum efficiency, $\overline{QE}$, to be 17%. For Neon the simulation predicts an average of 50 photons per electron. Taking 80% of the $\overline{QE}$ times the 50 photons per event, we get 6.8 photoelectrons, essentially the same as that listed in Table 2.

As a further check we have compared the estimates in Table 2 with past work. Ref. [4] provides (as have others) a simple formula based on their experience[3]: $N_{\rm pe} = 150L({\rm cm})\theta_c^2$. For Neon at 1 Atm $\theta_c = \cos^{-1}(\frac{1}{\beta n}) = 11.6\,{\rm mrad}$. For a 240 cm active length this suggest 4.8 PE's. Readers should note that the estimates in Table 2 are for the case when the tank is filled with 1 ATM of Neon. For comparison, when filled with Argon at 1 ATM (for pions below 6

[3]The authors' [4] calculation, taking wavelengths between 200 and 500 nm, assuming a 25% photo-cathode efficiency and 80% light collection efficiency, is considerably higher: $N_{\rm pe} = 275L\theta_c^2$.

GeV) the $N_{\rm pe}$ is more than 4 times larger.

4.1 Wavelength shifter

Although UV glass windows are transparent down to approximately 200 nm, second only to the prohibitively expensive quartz windows, the measured mirror reflectivity extends much farther into the ultraviolet; as indicated in Figure 2, the reflectance is 79% at 150 nm, down only 8% from its asymptotic value of 87% in the visible region. To make a better match between the phototube spectral sensitivity and the mirror reflectivity, therefore, a 25 kÅ (2500 nm) layer of the wavelength shifting material para-Terphenyl covered by 25 nm of MgF will coat the phototube entrance windows. The para-Terphenyl absorbs light in the UV and retransmits in the range of 390 nm. It has been shown that this improves the response by a factor of two and makes them superior to the PMT's with quartz windows[5]. Adopting this approach for the SHMS Čerenkov allows us to expect that, on average, 10 photoelectrons will be produced when using 1 Atm of Neon.

5 Optics Layout

The detector has to have an active area of 70 cm in the dispersive and 80 cm in the transverse directions. Very large mirrors are difficult to obtain so we have settled on four mirrors (the HMS Cerenkov uses two mirrors), each focusing on a separate PMT. To cover the active area of the scattered beam envelope each need to be approximately 40 by 40 cm. In order to move the focus outside the active area the mirrors have to be tilted and have a focus long enough to limit the tilt angle in order to minimize the spot size. Simple algebra tells us that the mirrors should have a radius of curvature in excess of 100 cm and smaller than 200 cm.

To further understand the needs of the optics of the detector, a program to ray trace the light through the detector was used[4]. This program used as input the placement of the mirrors and PMTs along with the output of TRANSPORT. This TRANSPORT output was the first and second order matrices for the particle trajectories after the focusing and bending magnets in the SHMS[6]. Thus, we were able to simulate the particles and the Čerenkov light they produced as the particles traversed the detector. The front of the SHMS Čerenkov is located 310 cm before the focal plane or 15 m from the target. At the end of the 2.5 m long tank the acceptance coverage is from $(-25, +45)$ cm in the vertical and $(-40, +40)$ cm in the horizontal along the central ray[7]. Note that in the coordinates system used here z is along the particle direction, positive y is to the left and positive x is in the direction of increasing momenta, or down.

Providing the raytrace code with reasonable starting positions for the mirrors and their tilt angles is not straightforward but with some effort a bit of

[4]Originally written by former UVa student N. Phillips for the HMS Čerenkov.

intuition can be gained. Nonetheless, as we have learned, it provides an excellent starting point for more sophisticated simulations, even though it is strictly 2D and averages over the missing dimension. Figure 5 is the output of the code for the dispersive direction. In this figure, the solid black lines represent the electron trajectories and the dotted cyan lines the limits of the Čerenkov light cone about each particle. The red dotted lines are the photons path after they have reflected from the mirrors. For a radius of curvature $\rho = 155$ cm, tilt angle of $\approx 15^\circ$, $\Delta\theta = \pm 55$ mr and a $\frac{\delta p}{p} = (-10, +20)$ the PMTs can be placed outside the active area such that 98% of the photons reflected from the mirrors can be focused on the 120 mm PMT face.

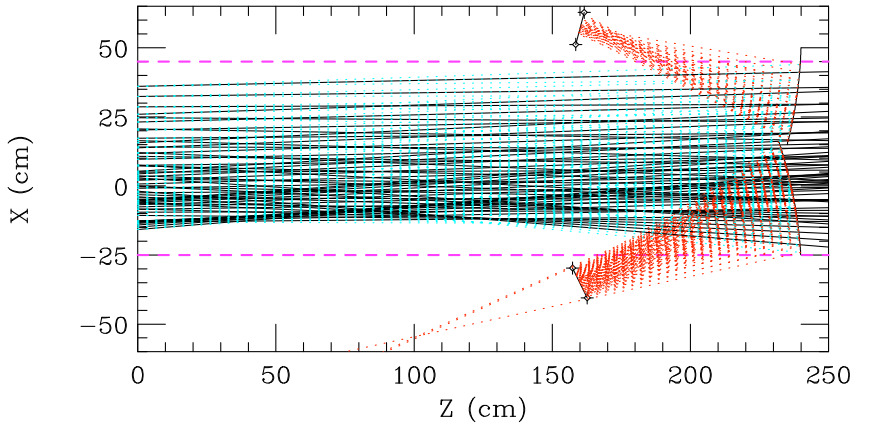

Figure 5: Output of raytrace program for the dispersive direction for two mirrors each with a radius of curvature $\rho = 155$ cm, a tilt angle of $\approx 15^\circ$, $\Delta\theta = \pm 55$ mr and a $\frac{\delta p}{p} = (-10, +20)$. This simulation indicates that 98% of the light will be collected on the PMT face. The thick dashed line indicates the active area of the detector.

5.1 Geant4 simulation

In order to refine the analysis of the optics a Geant4 simulation of the detector was written by UVa graduate student Vahe Mamyan. This code exploits the 3D and visualization power of modern computing and the physics built into Geant4. The geometry of the detector can be defined almost arbitrarily and the mirrors placed with independent tilt angles and radii of curvature. The set of vectors describing the electron rays can come from a random selection across the acceptance (as in the raytrace program mentioned above) or from a

set of vectors produced by a CODA analysis of the SHMS[7]. The generated photons positions (x, y, z) are recorded at a set of virtual 'planes' in front of the initial PMT locations and their distribution be studied to determine the optimal location for the PMTs, given a radius of curvature and tilt angle for the mirrors. In the left side of Figure 6 shows the geometry of the detector in the simulation and, in the right panel a single event (an electron radiating Cerenkov photons).

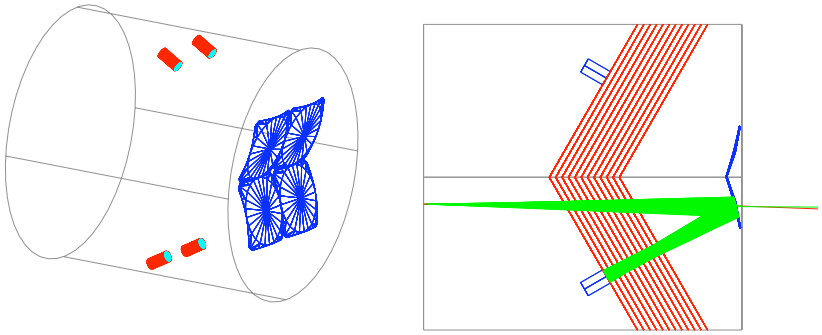

Figure 6: Left: A view of the geometry of the Geant4 simulation of the SHMS Noble gas Cerenkov. Four mirrors are placed at one end of the 2.5 m long tank, each focusing on a PMT. Right: A sample event from the simulation. The red lines are the virtual planes where the positions of the photons are recorded.

We ran the simulation with argon in the tank for a wide variety of mirror radii and tilt angles and found that the results of the raytrace program were confirmed. With mirror radii of 155 cm and a tilt angles of 15° 99% of the photons striking the mirrors were collected on the 120 mm PMT face. Using the position information recorded at the planes and at the mirrors we could also see which areas on the mirrors were the source of lost photons. The data were analyzed by first determining the position (x, y, z) at each plane (and for each mirror). Then a circle of diameter 120 mm was centered on the mean of those locations. The data set was reanalyzed and each photon was subject to the cut that they pass within that diameter. These were counted as successes. When a photon failed this cut its location on the mirror was plotted. Plane 6 is the ideal location for the PMT and there 99% of the photons were collected. It is gratifying to see in Figure 9, that the spot size was smaller than the PMT diameter. Some other results of the simulation are seen in Figures 7 and8 below.

The efficiency results seen against plane number has a broad maximum. In order to better define the optimal location we analyzed the analyzed the simulated data with a PMT size of 60 mm diameter. While returning a lower collection efficiency (as to be expected) we found the maximum to be at approximately 165 cm from the front of the Cerenkov tank. See Figure 10.

The simulation run under the same conditions but with neon gas confirms

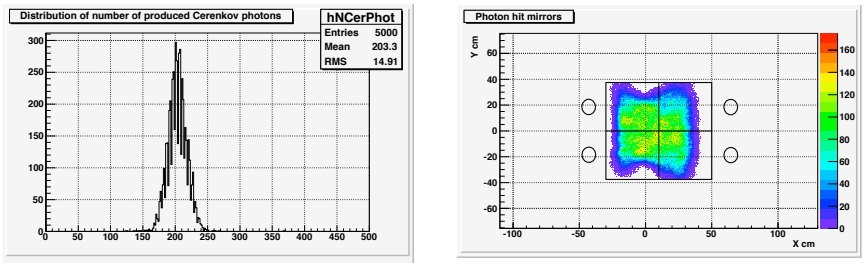

Figure 7: Left: From a 5000 event sample of electrons the distribution of the number of photons per electron. The right panel gives the distribution of those photons on the mirrors.

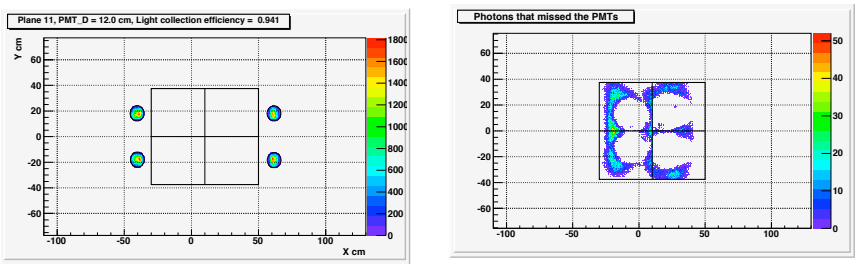

Figure 8: Left: For plane 11 out of 15 (with 1 being closest to the PMTs). This is NOT the ideal position for the PMT. It is given as an example. The left panel shows the distribution of the photons on the face of the PMTs. The right panel gives the distribution of the photons (on the mirrors) that did not survive the cut of passing through the 120 mm diameter. Note that essentially all the photons that reflected from the center of the mirrors passed the cut and those at the extremes were more likely to fail.

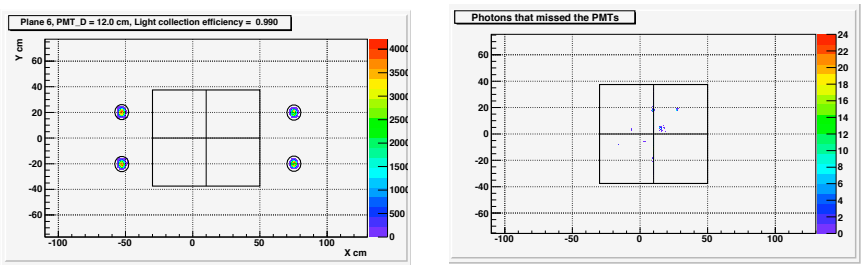

Figure 9: Left: For plane 6 (approximately 165 cm from the front of the detector) the distribution of photons on the face of the PMTs. This IS the ideal position for the PMTs. The efficiency here was 99%. The right panel gives the distribution of the photons (on the mirrors) that did not survive the cut of passing through the 120 mm diameter.

what is to be expected - fewer photons by a factor of 4 and a significantly smaller spot on the PMT face. It is well known that collection efficiency in a PMT falls as the photon moves away from the center of photocathode. Photons from Neon are more tightly focused and this should moderate somewhat the difference in the N_{pe} between the 2 gases. Further work on the simulation should confirm this. See Figure 11.

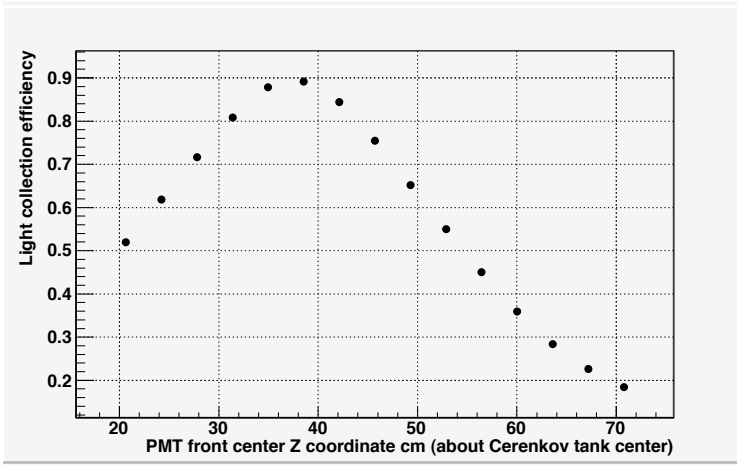

Figure 10: Maximum collection efficiency is found to be 38 cm from the tank center or 163 cm from the front of the tank. This was run with a 60 mm diameter PMT (cut), not the planned 120 mm.

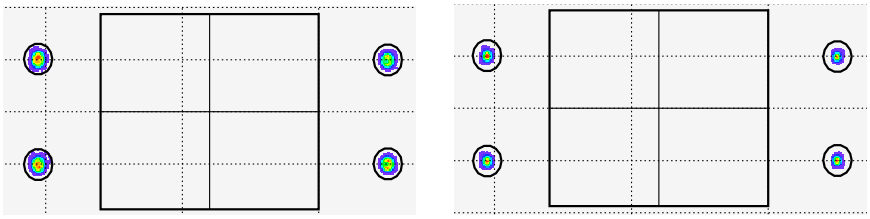

Figure 11: Comparison of spot size at PMT face for Argon (left) and Neon (right). A smaller spot size and a reduced number of photons from Neon is a consequence of its smaller index of refraction n.

6 Knock-on electrons

One of the major sources of background in a Čerenkov detector comes from $\delta-$rays, also known as "knock-on" electrons. If, during its passage through the detector array, a below threshold primary particle knocks an atomic electron free with sufficient energy to produce Čerenkov radiation, then the primary particle will be falsely registered in the detector.

Energy and momentum conservation gives the energy of the knock-on electron as $E' \simeq 2m_e \frac{p_\pi \cos(\theta)^3}{M_\pi^2 + p_\pi^2 \sin(\theta)^2}$ [9] where θ is the angle of the electron relative to the particle trajectory. Notice that as $\theta \to \pi/2$, the knock-on energy tends to the electron rest mass, $E' \to m_e$. In this limit, the pion is scattered at very small forward angles where the Coulomb singularity drives the cross section to infinity. Therefore, knock-on electrons will be produced most abundantly, but with the least energy, at right angles to the track of the primary particle. Collision probabilities for these processes are covered in [8] among others and by estimating these probabilities, we can get the pion rejection rate for the detector.

Here we follow Ref. [9] and to a lesser extent Ref. [10] and introduce the

following functions:

- $\phi(E, E')$ - the probability for an incident particle of energy E producing a knock-on electron of energy E', per unit energy, per unit path length;
- $\bar{N}(E, E', s)$ - the mean number of photoelectrons produced by a knock-on electron of energy E' at a point s along the π^-'s path. The energy E of the incident π^- determines the angle of the electron with respect to the π^-'s path, and thus the length of the electron's path;
- $\epsilon_N(\bar{N})$ - the probability that the PMT circuitry registers $\bar{N}$ photoelectrons when the threshold is set to N. See the Appendix.

We also have the two energies:

- E_{th} - the threshold energy for electrons to produce Čerenkov radiation;
- E_m - the maximum transfer energy for the pion-electron collision.

Using these functions and energies[5], we can write down the efficiency for detecting a knock-on electron produced by an incident π^- as the probability for producing a knock-on multiplied by the probability of registering the knock-on electron, or as the integral

$$\epsilon_{ko} = \int_{E_{th}}^{E_m} \int_0^L \phi(E, E')\epsilon_N(\bar{N}(E, E', s))dsdE'; \tag{11}$$

where

$$\begin{aligned}
\phi(E, E') &= 2\rho C \frac{m_e}{\beta} \frac{1}{E'^2} \left(1 - \beta^2 \frac{E'}{E_m}\right), \\
\bar{N}(E, E', s) &= A \frac{L - s}{\cos\theta(E, E')} \left(1 - \frac{1}{\beta'^2 n^2}\right), \\
E_{th} &= \frac{nm_e}{\sqrt{n^2 - 1}}, \\
E_m &= 2m_e \left(\frac{p}{m}\right)^2, \\
\cos\theta(E, E') &= \frac{1}{\beta}\sqrt{\frac{\gamma' - 1}{\gamma' + 1}}, \\
C &= 0.15\frac{Z}{A}.
\end{aligned} \tag{12}$$

Since the only way the type of material appears in the above equation is as a constant factor of $\rho Z/A$, we can define the electron density $\rho_e \equiv \rho Z/A$ and use this to normalize the knock-on probability to get $\epsilon^o_{ko} = \epsilon_{ko}/\rho_e$. This allows us to calculate the knock-on probability but once.

This integral is handled numerically, and is dependent on E, the incident π^- energy; N, the detector threshold and A, the detector efficiency factor. ϵ^o_{ko} is

[5]The primed quantities refer to the knock-on electron, the unprimed to the incident pion.

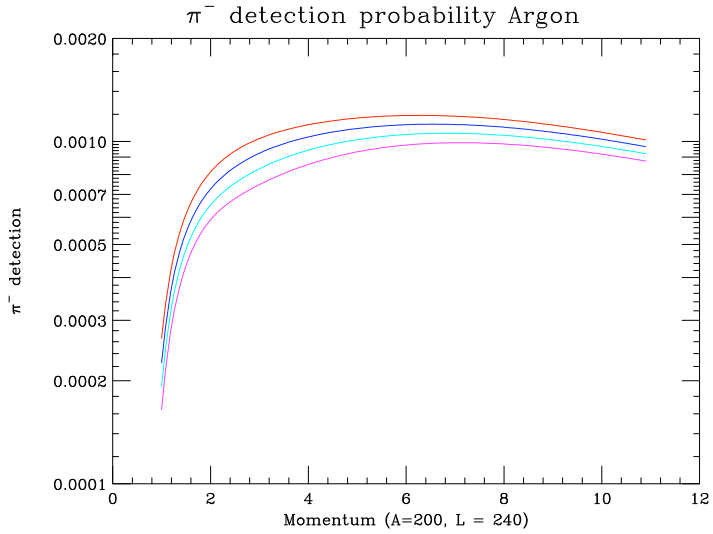

Figure 12: Pion detection probability rate for Argon at 1 Atm, versus momentum for a fixed A (see Section 4) and tank length L. The colored lines from top to bottom are for increasing PE threshold, from 1 to 4. The SHMS Noble Gas Cerenkov should provide a pion rejection of 1000:1.

the probability to "detect" a pion due to knock-on noise and Figure 12 shows ϵ^o_{ko} for Argon at 1 ATM as a function of the π^- momentum and fixed A. Figure 12 tells us that, as we would expect, the rejection rate $(1/\epsilon^o_{ko})$ gets worse the higher the incident momentum. We also see that the higher the threshold N, the better the rejection rate. These results indicate, for the worse case of Argon, that the detector will provide something better than 1000:1 rejection.

7 Knock-on electrons from front window

An estimate of the knock-ons generated in the front window of the tank can also be made using the prescription of Section 6. The task becomes easier however. First, $\bar{N}$ is now constant as all the knock-ons are produced in the front window and the effective radiator length is constant – 240 cm, and in fact is the same for a normal electron, i.e.: $\bar{N} = AL(1 - 1/\beta^2 n^2)$. Secondly, since $\bar{N}$ is constant, so is $\epsilon_N(\bar{N})$. Thus, for aluminum, we have

$$\frac{d\epsilon_{\rm ko,window}}{ds} \simeq 1 \times 10^{-5} \text{per mil.} \tag{13}$$

A 4 mil thick window the will make a negligible additional contribution to the knock-ons detected.

8 Tank Design

The mechanical design of the tank is not especially challenging given that the tank will only operate at 1 ATM. It must be of the required length and breadth of the beam envelope and must provide a mounting and alignment mechanisms for both the mirrors and the PMTs. The end windows can be of very thin material ($\approx$ 0.004 inches of Al). There must also be lifting hooks and an assembly to allow it to be held on the rails of the SHMS detector hut. The tank must include feedthroughs for HV and signal cables, a set of small ports for temperature and pressure transducers and a connection to the gas supply.

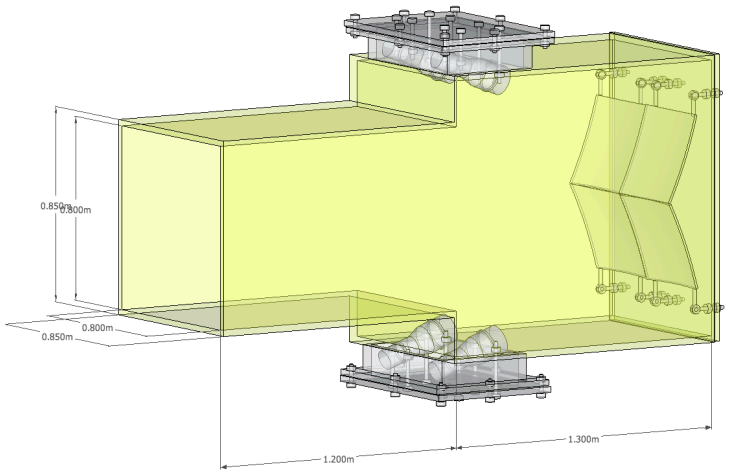

Figure 13: A sketch of the tank. Since it must only operate at 1 Atm, the main demands are that it be of the correct dimensions, be light tight, leak tight , and allow for the PMT and mirror positions be adjustable, secure and reproducible.

9 Filling the tank

The process of filling by dilution (or repeated filling) is necessary as the tank is not currently being designed to go to overpressure. It is easy to show that with an initial atmosphere P_0 of air, after filling to a gauge pressure P and purging back to atmosphere n times, the partial pressure P_n of the remaining air is:

$$P_n = P_0 \left(\frac{P_0}{P_0 + P} \right)^n .$$

The partial pressure of the oxygen remaining in the tank is simply 21% the atmospheric abundance, of the value calculated above.

The oxygen absorption cross section[11], $\sigma_{\rm abs}$, at 200 nm is $10^{-23}{\rm cm}^2$. Hence we can calculate the intensity fall off using this and the following relation,

$$I = I_0 e^{-\frac{x}{L}}$$

where $L = \frac{2A}{N_A \rho \sigma_{\rm abs}}$. A is the atomic number of oxygen, 2 accounts for the fact that it is a molecule and ρ is its density and N_A is Avogadro's number.

We find that in 1 Atm of air the absorption due to oxygen would reduce the intensity of light (at 200 nm) to $\frac{1}{e}$ in $\frac{3800}{0.21} \approx 18,100$ cm or more than 70 times the length of the tank. Transmission through the UV glass of the R1584 is limited to about 200 nm but, as mentioned earlier, the application of a wavelength shifter can move the short wavelengths to better match the glass and the PMT sensitivity. Hence we should worry about the absorption at smaller λ. At 170 nm the oxygen absorption cross section is four orders of magnitude higher and the absorption length is only 0.38 cm. Using the expression above and a filling a gauge pressure of 0.1 Atm. we discover that 30 tank volumes must be flowed through the tank to reduce the partial pressure of oxygen to 1% which would still mean a significant absorption at 170 nm. Not only is this painful, but when neon is used, it might be very expensive. Better ideas have been implemented[12]. This involves first purging from the bottom of the tank with CO_2. Then the Cerenkov gas (neon in the case discussed) was added to the tank while the CO_2 was frozen out with liquid nitrogen cooled freezer. Passing the tank gas through the freezer multiple times could reach the desired contaminate level.

Neon gas is not toxic at normal temperature and pressure. However, neon is a simple asphyxiant. It can displace oxygen in the air, especially in a confined space such as the detector hut. Hence when filling, the gas must be vented out of the hall. Additional measures (oxygen deficiency alarms) must be taken to protect personnel working in the detector hut in the event that the tank should rupture.

10 Acknowledgements

Much of this work drew from the experience designing and building the HMS Cerenkov. The work of former UVa students Nicholas Phillips and Chris Cothran was extremely useful. Vahe Mamyan was responsible for the Geant4 simulation. Garth Huber and Howard Fenker made important contributions. Thanakorn Iamsasri drew the sketch of the tank and provided some of the analysis of the simulated data.

References

[1] J. D. Jackson, *Classical Electrodynamics, 2nd Edition.*

[2] Richard Fernow, *Introduction to experimental physics.*

[3] http://www.matweb.com/search/datasheettext.aspx?matguid=a4736834d783413fb20601849248f115

[4] R. L. Anderson and J. Grant, "Differential Cherenkov Counters For Use At High Momenta," Nucl. Instrum. Meth. **135**, 267 (1976).

[5] E. L. Garwin, Y. Tomkiewicz and D. Trines, *Method For Elimination Of Quartz Face Phototubes In Cherenkov Counters By Use Of Wavelength Shifter*, Nucl. Instrum. Meth. **107**, 365 (1973).

[6] This matrix was generated by Chen Yan and communicated to me via T. Horn.

[7] http://www.jlab.org/~hornt/HALLC_12GEV/shms_beam_envelope.html

[8] B. Rossi, *High Energy Particles*, Prentice Hall, Third Printing, 1961.

[9] A. S. Vovenko, et. al., *Gas filled Čerenkov counters*, Usp. Fiz. Nauk. **81**, 453-506.

[10] J. A. Lezniak, *Average added component of Čherenkov radiation due to knock-on electrons*, Nucl. Instrum. Meth. **136**, 299-306.

[11] M. Ogawa, *Absorption Cross Sections of O_2 and CO_2 Continua in the Schumann and Far-UV Regions*, Jour. Chem. Phys. **54** 2550-2556.

[12] J. Engelfried *et al.*, *The RICH detector of the SELEX experiment*. Nucl. Instrum. Meth. A **433**, 149 (1999).

A Detector Efficiency

Here I am following Ref. [9]. We are interested in the question of given $\bar{N}$ $(= N_e)$ photoelectrons, what is the probability of registering the incident particle. We can assume that the photoelectrons have a Poisson distribution

$$W(N, \bar{N}) = \frac{\bar{N}^N e^{-\bar{N}}}{N!} \tag{14}$$

for registering N photoelectrons when $\bar{N}$ are expected. If by $P(N)$ we denote the probability for the detector (PMT and associated circuitry) to record the pulses due to N photoelectrons, we can write the efficiency of the detector as

$$\epsilon = \sum_{N=0}^{\infty} W(N, \bar{N}) P(N). \tag{15}$$

Let us assume that $P(N)$ is of the form

$$P(N') = \begin{cases} 0, & N' \leq N-1; \\ 1, & N' \geq N. \end{cases} \tag{16}$$

i.e.: there is a threshold for the detection of N photoelectrons. Then the efficiency is of the form

$$\epsilon = 1 - e^{-\bar{N}} \left(1 + \sum_{N'=1}^{N-1} \frac{\bar{N}^{N'}}{N'!} \right). \tag{17}$$

Hence, we have the efficiency functions

$$\begin{aligned} \epsilon_1 &= 1 - e^{-\bar{N}}, \\ \epsilon_2 &= 1 - e^{-\bar{N}}(1 + \bar{N}), \\ \epsilon_3 &= 1 - e^{-\bar{N}}(1 + \bar{N} + \bar{N}^2/2), \\ \epsilon_4 &= 1 - e^{-\bar{N}}(1 + \bar{N} + \bar{N}^2/2 + \bar{N}^3/6), \\ &\text{etc.} \end{aligned} \tag{18}$$